Kinetics of the NH_2 + NO Reaction: Effects of Temperature on the Total Rate Constant and the OH/H_2O Branching Ratio

Eric W. Diau, Tao Yu, Marlyn A. G. Wagner,† and M. C. Lin*

Department of Chemistry, Emory University, Atlanta, Georgia 30322

Received: December 27, 1993®

The rate constant for the reaction of NH_2 with NO has been measured between 297 and 673 K using the cavity-ring-down technique to monitor the disappearance of the NH_2 radical. The measured bimolecular rate constant can be effectively represented by the expression $k^{II} = (2.2 \pm 0.7) \times 10^{-12} \exp[525 \pm 80)/T]$ cm^3/s, which agrees reasonably well with the results of several other recent measurements employing various diagnostic methods. A multichannel RRKM calculation has been carried out to account for the observed negative temperature dependence and the product branching ratio, OH/H_2O, based on Walch's recent potential energy surface data for various transition states and stable intermediates leading to the formation of the OH and H_2O products. The predicted temperature dependencies agree reasonably well with experimental observations. We have also performed kinetic modeling using a set of of reactions involving H, NH_3, NH_2, NO, and their anticipated products. The result of the modeling aided by sensitivity analysis suggests that the unknown "third channel" responsible for the decline of the $([OH] + [H_2O])/[NH_2]_0$ ratio at high temperatures (ref 23) may result from secondary reactions which produce neither OH nor H_2O. These reactions include $NH_2 + H \rightarrow NH + H_2$ and $NH_2 + NH_2 \rightarrow NH + NH_3$.

Introduction

The reaction of the NH_2 (amidogen) radical with NO plays a significant role in both atmospheric chemistry[1,2] and the combustion process related to NO_x formation and removal.[3-6] In the thermal de-NO_x process,[4,5] nitric oxide emission from engine exhaust is reduced by addition of ammonia into the flue gases at combustion temperatures at which a significant amount of NH_2 can be generated. Additionally, the NH_2 radical, produced from the OH + NH_3 reaction in the troposphere, reacts with NO, providing a significant disappearance pathway for the atmospheric NO.

There have been many kinetic studies of this reaction with various techniques.[7-23] The absolute rate constants from room-temperature measurements have a wide range of values, varying from 8.3×10^{-12} to 2.7×10^{-11} cm^3/s. The values of the overall rate constant obtained by the flash photolysis technique are generally 2 times greater than those obtained by the discharge flow method. No pressure dependence of the rate constant for NH_2 + NO was observed in all previous investigations. Thus, there is no obvious cause for the discrepancy in the rate constant except perhaps systematic errors. Furthermore, all experimental studies of temperature effect[10-13,20,21] on the rate constant reveal a negative dependency.

Based on the products monitored by experiments,[12-14,18-21,23] two major channels contributing to this reaction have been proposed:

$$NH_2 + NO \rightarrow H_2O + N_2 \quad (1)$$

$$\rightarrow OH + N_2H \quad (2)$$

Reaction channel 1 produces two stable molecules, H_2O and N_2. In the reaction, three bonds in the reactants are broken and three whole new bonds are formed in the products. The OH radicals formed in the reaction channel 2 could feed a chain of reactions in the thermal de-NO_x process; thus, several kinetic modeling studies attempted to determine the branching ratio of OH (α; defined as k_2 divided by the overall reaction rate constant of NH_2 + NO). A value of α of 0.29–0.4 was required to reach agreement between kinetic model predictions and experimental measurements under combustion conditions.[24-28] The work of Kinball-Linne and Hanson[29] implies that α may vary with temperature from 0.48 at 1050 K to >0.8 at 1400 K.

Experimental measurements for α have ranged from 0.1 to $\geq$0.65 at room temperature,[12-14,18-21,23,30] but the recent investigations[18-21,23] converge on the smaller value of about 0.1. Three groups have measured the temperature dependence of α. Bulatov et al.[21] obtained a value of 0.2 for α at 620 K using a flash photolysis/intracavity laser spectroscopy technique. Atakan et al.[20] reported that α varied from 0.1 at 300 K to 0.19 at 1000 K using the laser photolysis/laser-induced fluorescence technique; they calibrated the OH signal intensity with the known OH yield from H_2O_2 photolysis. More recently, Stephens et al.[23] studied the OH branching ratio as well as the total yields of OH and H_2O from NH_2 + NO using the laser photolysis/infrared kinetic spectroscopy method by calibrating infrared absorption cross sections for key species at different temperatures. They obtained a value of 0.17 for α at 1173 K; they also found that the value of the total OH and H_2O yield falls off from 0.94 at 299 K to 0.7 at 1173 K. A possible "third channel," in addition to reactions 1 and 2, was proposed to interpret the observation. When the observed data were extrapolated to the combustion condition, both values of α measured in the latter two studies are too low to model the thermal de-NO_x process.

There have been several theoretical studies of potential energy surface (PES) for NH_2 + NO.[31-35] For example, Melius and Binkley[33] applied the fourth-order Møller–Plesset perturbation theory with bond-additivity corrections (BAC-MP4) to study the energetics of the reaction pathways and indicated that NH_2 + NO forms a stable intermediate H_2NNO, which can rearrange to form the products $H_2O + N_2$ or to form $OH + N_2H$ near thermoneutrally. Later, Harrison et al.[34] carried out a study for this system using MP2 through the MP4SDQ theory with a 6-31G* basic set and obtained a small energy barrier (3–4 kcal mol^{-1}) for reaction channel 1 and no barrier with respect to OH + N_2H, but having an endothermicity of 7.5 kcal/mol. Recently, Walch[35] used internally contracted configuration interaction (ICCI) calculations based on an (10/10) complete active space

† GIFT Fellow. Permanent address: South Gwinnett High School, Snellville, GA.

* To whom correspondence should be addressed.

® Abstract published in *Advance ACS Abstracts*, March 15, 1994.

0022-3654/94/2098-4034$04.50/0

self-consistent-field (CASSCF) theory to study the PES of this system. Qualitatively, the same results were obtained with larger basic sets and more extensive inclusion of electron correlation effects for both stationary point geometries and energies. The heat of formation for the product N_2H was also determined in these calculations with various theoretical methods,[31-45] giving values ranging from 45 to 79 kcal mol^{-1}. No direct experimental measurement has been reported for the heat of formation of the N_2H radical.

Earlier, Abou-Rachid et al.[32] have carried out an RRKM calculation of rate constant for the NH_2 + NO system based on a simple kinetic model. The calculated rate constant which decreases with temperature from 200 to 500 K is comparable to that determined experimentally at room temperature, but it deviates from the experimental observations above 700 K. Phillips[46,47] used an approximate semiclassical trajectory method to compute capture rates with a dipole–dipole + Morse potential, which were then combined with RRKM rates for passing through entropy bottlenecks on the PES for reaction 1. This calculation was based on the PES calculated by either Melius and Binkley[33] or Harrison et al.,[34] but no structural parameters for the radical–radical transition state (H_2N···NO) were available from previous theoretical PES calculations.

We have carried out a study of the NH_2 + NO system using laser photolysis coupled with the cavity-ring-down (LP/CRD) method. A multichannel RRKM calculation was applied to simulate the effect of temperature on both the total rate constant and the product branching ratio, OH/H_2O. Kinetic modeling was performed in conjunction with sensitivity analyses to investigate the complicated effect of secondary reactions on experimentally reported branching ratios and on the genesis of the "third channel" postulated by Stephens et al.[23]

Experimental Section

The experiments were carried out in a heatable Pyrex glass reactor wrapped with heating tape to attain a desired temperature. The NH_2 radicals were generated by pulsed-laser photolysis of NH_3 at 193 nm and detected by the cavity-ring-down method at 537.6 nm. The details of the technique and the experimental setup have been described previously;[48,49] hence, only a summary is given here.

An ArF laser (Lambda Physik, LPX 100) was utilized to photolyze NH_3. After a certain delay, a second probing laser beam (Laser Photonics N_2 laser pumped dye laser with Coumarin 540A dye at λ = 537.6 nm) was introduced through one of two highly reflective mirrors (R = 0.9999 at 540 nm) enclosing the reactor. The two mirrors were optically aligned by a He–Ne laser to form a low-loss resonator. The concentration of NH_2 was measured in terms of the decay time of an injected dye laser pulse, detected with a photomultiplier tube (PMT, Hamamatsu 955) behind the second mirror. When the cavity was absent of NH_2, the photon decay time of probing laser pulse (t_c^0) was increased significantly from its original 8 ns to about 30 μs (here the fall time was measured for the duration of 10–90% I_0, where I_0 was the initial pulse height) due to oscillation inside the cavity. In the presence of NH_2, the decay time of the probing laser pulse will decrease from t_c^0 to t_c. These photon decay times are related to the NH_2 radical reaction time, t', according to the following equation[48,49]

$$\ln(1/t_c - 1/t_c^0) = B - k^I t' \qquad \text{(I)}$$

where B is a constant depending on NH_2 absorption coefficient, initial concentration, and cavity properties. k^I is the pseudo-first-order decay constant of NH_2. Experimentally, t' is the delay time between the photolysis and probing laser pulses.

The photon decay times, t_c and t_c^0, were measured with the photolysis laser turning on and off, respectively, and were recorded by a digital storage oscilloscope (LeCroy 9310M). In the absence of NO, a wavelength scan carried out between 536 and 539 nm revealed a strong absorption peak at 537.6 nm, corresponding to the band head of the $\tilde{A}^2A_1(1,7,0) \leftarrow \tilde{X}^2B_1(0,0,0)$ vibronic transition of the NH_2 radical. For kinetic measurement, the probing dye laser was fixed at 537.6 nm with t' varying from 30 μs to 3 ms depending on the concentration of the NO used. The triggers for lasers and oscilloscope were generated by a pulse generator (Stanford Research, DG535) which was controlled by a microcomputer.

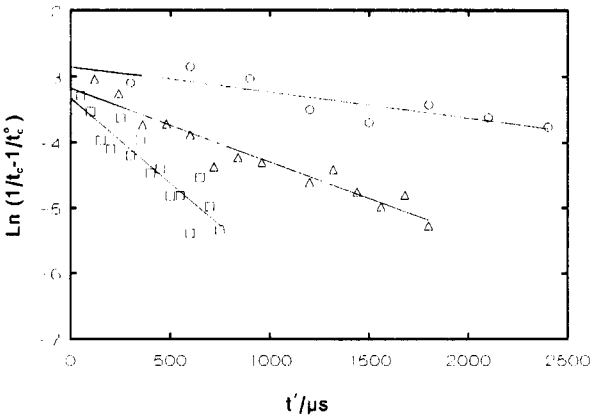

Figure 1. Typical pseudo-first-order decay of NH_2 for various concentrations of NO at T = 523 K, P = 50 Torr: (○) [NO] = 0; (△) [NO] = 1.80×10^{14}; (□) [NO] = 4.78×10^{14}, all in units of molecules/cm^3.

All experiments were carried out under slow-flow conditions using typically 50 Torr of Ar as buffer gas. The Ar (99.9995%) was used without further purification. The radical source, NH_3, was purified by standard trap-to-trap distillation. Reactant NO (99%) was purified by vacuum distillation through a silica gel trap maintained at 195 K to remove impurities such as NO_2. The concentrations of NO and NH_3 were determined from measurements of their mass flow rates using calibrated mass flowmeters (Hastings and MKS) and the total pressure, measured with an MKS Baratron manometer.

Typical experimental conditions were as follows: total flow rate F_T = 10–17 STP cm^3 s^{-1}; total pressure P = 20–150 Torr; reaction temperature T = 297–673 K; [NH_3] = (0.6–7.6) × 10^{15} molecules cm^{-3}; [NO] = (2–65) × 10^{13} molecules cm^{-3}; $[NH_2]_0 \approx (1–5) \times 10^{12}$ molecules cm^{-3}; time delay between the photolysis laser and the probe laser t' = 30 μs–3 ms.

Results

The reaction was studied under pseudo-first-order conditions with [NO] ≫ [NH_2]. Thus, the reciprocal difference between the probe laser decay time with and without NH_2 is expected to exhibit a simple exponential decay with respect to reaction time according to eq I. Figure 1 shows some typical semilog plots of $(1/t_c - 1/t_c^0)$ vs reaction time for various concentrations of NO at 523 K. The pseudo-first-order rate constant k^I was determined from the slope of such a decay plot for each [NO]:

$$k^I = -\mathrm{d}\ln(1/t_c - 1/t_c^0)/\mathrm{d}t \qquad \text{(II)}$$

The observed absolute values of the second-order rate constant (k^{II}) for the NH_2 + NO reaction, summarized in Table 1, were obtained from the slopes of k^I vs [NO] plots, as illustrated in Figure 2 for 523 K. Figure 3 summarizes these second-order rate constants in the Arrhenius form, together with the results of other measurements. A least-squares fit of our 13 data points between 297 and 673 K to the Arrhenius equation yielded

$$k^{II} = (2.2 \pm 0.7) \times 10^{-12} \exp[(525 \pm 80)/T] \quad cm^3/s$$

in which the uncertainties represent one standard deviation.

TABLE 1: Summary of Measurements of the Rate Constant for the Reaction $NH_2 + NO$

T/K	P/Torr	$[NO]/10^{14}$ cm^{-3}	$[NH_3]/10^{15}$ cm^{-3}	$k^{II}/10^{-11}$ cm^3 s^{-1}
297	50	1.5–6.5	2.8–4.4	1.43 ± 0.08[a]
	50	0.9–5.0	1.3–2.2	1.46 ± 0.07
315	50	0.6–3.0	3.8–4.6	1.02 ± 0.12
333	50	0.8–5.0	5.4–7.6	0.91 ± 0.06
353	50	0.8–3.5	1.4–1.9	1.10 ± 0.12
373	51	0.8–6.0	1.3–1.9	0.71 ± 0.06
383	50	0.4–3.0	2.5–3.6	1.06 ± 0.09
423	20	0.4–2.5	0.6–0.9	0.83 ± 0.08
	50	0.7–5.0	5.8	0.75 ± 0.04
	100	0.6–5.0	1.2–1.8	0.70 ± 0.04
	150	0.6–6.0	1.1	0.68 ± 0.05
473	57	0.9–5.0	1.1–1.8	0.79 ± 0.10
500	50	0.4–3.5	2.7	0.67 ± 0.05
523	50	0.5–5.0	2.9–3.8	0.51 ± 0.02
573	50	0.6–4.5	1.3–3.5	0.61 ± 0.04
623	50	0.2–3.0	0.8–1.6	0.59 ± 0.05
673	50	0.6–5.5	2.0–2.2	0.37 ± 0.03

[a] The uncertainties represent one standard error.

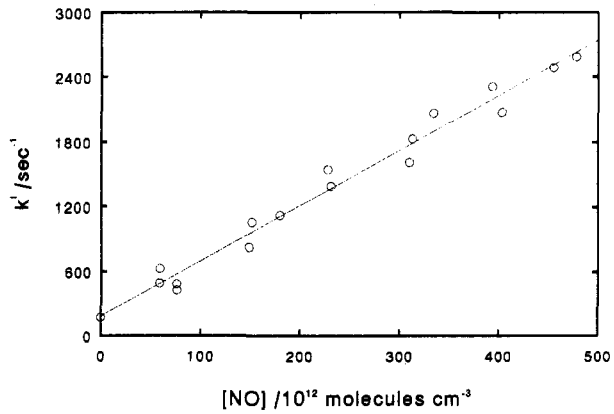

Figure 2. Typical plots of the pseudo-first-order decay rate k^I against NO concentration at 523 K.

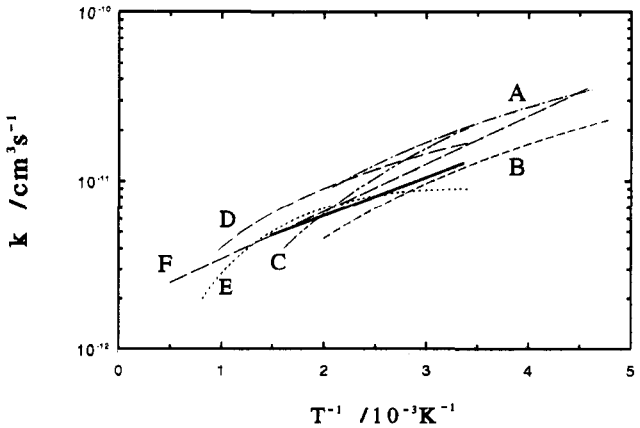

Figure 3. Arrhenius plot for the total rate constant for the $NH_2 + NO$ reaction: (A) Stief et al.,[13] (B) Hack et al.,[11] (C) Bulatov et al.,[21] (D) Atakan et al.,[20] (E) Silver and Kolb,[12] (F) recommended by Baulch et al.[57] Our result is represented by the thick solid straight line. The data presented by Lesclaux et al.[10] overlap with curve D in the temperature range 300–500 K.

Discussion

Table 2 is a summary of the data shown in Figure 3. Our results (shown as the solid line in Figure 3) are in good agreement with previous studies, all exhibiting a negative temperature dependence. We have also studied the effect of pressure by varying it from 20 to 150 Torr at 473 K; no obvious change was observed in this test (see Table 1), which is consistent with previous observations as mentioned in the Introduction. A theoretical study by Phillips[47] reveals that the intermediate complex (NH_2-NO) has a lifetime of the order of 10^{-11} s at room temperature, which accounts for the observed absence of pressure effect on the rate constant. The result of our multichannel RRKM calculation, discussed in detail below, also supports that conclusion.

A. Multichannel RRKM Calculation. Based on previous theoretical work,[33-35] the reaction of NH_2 and NO forms the vibrationally excited intermediate NH_2NO, which may undergo a 1,3-hydrogen migration with an energy barrier of about 30 kcal mol^{-1} to give a trans–cis HNNOH isomer (trans about the NN bond and cis about the NO bond). The trans–cis HNNOH may isomerize along either the NN bond to form cis–cis HNNOH or the NO bond to form trans–trans HNNOH. Both isomers may also isomerize along either the NO bond or the NN bond to form cis–trans HNNOH, which may further decompose exothermically with an energy barrier of about 20 kcal mol^{-1} to form H_2O and N_2. Each HNNOH isomer may also decompose to produce OH and N_2H endothermically with a barrier of about 45 kcal mol^{-1}. The energy barrier for isomerization with respect to the NO bond is about 10 kcal mol^{-1}, which is much smaller than those with respect to the NN bond (about 40 kcal mol^{-1}); thus, the omission of the former isomerization step in our calculation should be a reasonable assumption. The multichannel RRKM calculation for the $NH_2 + NO$ reaction was performed simply by using the following mechanistic scheme

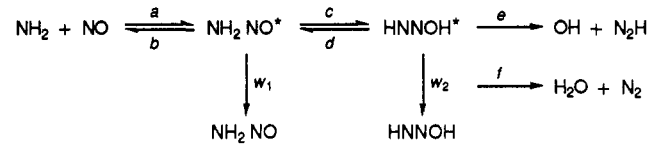

where the asterisk represents internal excitation. In the above scheme, we also assume that HNNOH dissociates to form H_2O and N_2 immediately after passing through the energy barrier of isomerization about the NN bond. The simplified potential energy diagram for the RRKM calculation is shown in Figure 4, which is depicted by the solid curves in accordance with Walch's theoretical results.[35]

The RRKM formulation for the chemically activated multichannel processes has been derived to give thermally averaged rate constants for individual channels, as described previously.[50,51] The thermally averaged bimolecular rate constant for each pertinent channel can be evaluated with a Boltzmann average of the energy-specific branching reaction probability by steady-state treatment for both NH_2NO^* and $NHNOH^*$ which gives rise to the following equations:

$$k_{OH}(T) = Q\int_0^\infty \frac{k_e(E)\,A(E)\,f(E^\ddagger)\,dE^\ddagger}{B(E)} \qquad \text{(III)}$$

$$k_{H_2O}(T) = Q\int_0^\infty \frac{k_f(E)\,A(E)\,f(E^\ddagger)\,dE^\ddagger}{B(E)} \qquad \text{(IV)}$$

$$k_{w_1}(T) = Q\int_0^\infty \frac{w_1 f(E^\ddagger)\,dE^\ddagger}{B(E)} \qquad \text{(V)}$$

$$k_{w_2}(T) = Q\int_0^\infty \frac{w_2 A(E)\,f(E^\ddagger)\,dE^\ddagger}{B(E)} \qquad \text{(VI)}$$

where

$$Q = \frac{1}{h}\frac{Q_{tr}^\ddagger}{Q_{NH_2}Q_{NO}}e^{-E_a^0/RT}$$

TABLE 2: Summary of Reported Arrhenius Parameters for NH_2 + NO Reaction

A^a	B^a	E^a	T/K	P/Torr	carrier gas	method[b]	reference
2.1×10^{-8}	−1.25	0	300–500	2–700	N_2	FP/RA	Lesclaux et al.[10]
4.5×10^{-7}	−1.85	0	209–500	0.4–4.0	He	DF/LIF	Hack et al.[11]
4.38×10^{-5}	−2.3	1360	294–1215	1.0–2.8	He	DF/LIF	Silver and Kolb[12]
2.77×10^{-7}	−1.67	0	216–480	2.5–20	Ar	FP/LIF	Stief et al.[13]
1.3×10^{-8}	−1.17	0	294–1027	3–100	N_2	LP/LIF	Atakan et al.[20]
5.6×10^{-6}	−2.2	0	295–620	1–31	N_2	FP/ILS	Bulatov et al.[21]
2.2×10^{-12}	0	−1043	297–673	20–150	Ar	LP/CRD	this work

[a] Arrhenius expression: $AT^B \exp(-E/RT)$, where A in cm^3 molecule^{-1} s^{-1} and E in cal mol^{-1}. [b] FP = flash photolysis; DF = discharge flow; LP = laser photolysis; LIF = laser-induced fluorescence; ILS = intracavity laser spectroscopy; CRD = cavity-ring-down.

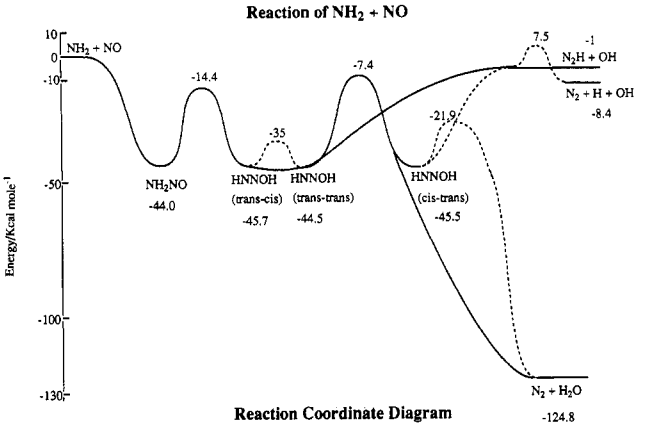

Figure 4. Potential energy surface diagram for the NH_2 + NO reaction based on the CASSCF/ICCI method calculated by Walch.[35] The dashed curves represent the processes which are not included in our RRKM calculation.

$$k_i(E) = \frac{Q_i^{\ddagger}}{Q_j}\sum P_i(E_i^{\ddagger})/hN_j(E), \quad i = b, c, d, e, \text{or } f; \quad j = 1 \text{ or } 2$$

$$A(E) = k_c(E)/[k_d(E) + k_e(E) + k_f(E) + w_2]$$

$$B(E) = k_b(E) + k_c(E) + w_1 - k_d(E)\,A(E)$$

$$f(E^{\ddagger}) = \sum P_b(E_b^{\ddagger}) \exp(-E_b^{\ddagger}/RT)$$

The observed overall rate constant for the disappearance of NH_2 in the presence of an excess amount of NO is given by the sum of individual thermal rate constants:

$$k_t(T) = k_{OH}(T) + k_{H_2O}(T) + k_{w_1}(T) + k_{w_2}(T) \quad \text{(VII)}$$

where k_{OH} and k_{H_2O} are the thermal rate constants for NH_2 + NO to form OH + N_2H and H_2O + N_2, respectively. The rate constants for stabilization of the excited adducts NH_2NO^* and $NHNOH^*$ are given respectively by $k_{w_1}(T)$ and $k_{w_2}(T)$; both are obviously functions of temperature and pressure. These rate constants are the effective quenching frequencies for both energetic intermediates, which were estimated with Troe's weak-collision approximation and expressed as $w_1 = \beta_1 Z_1[M]$ and $w_2 = \beta_2 Z_2[M]$, respectively, where Z_1 and Z_2 are the Lennard-Jones collision numbers and β_1 and β_2 stand for the collision efficiencies.

In eqs III–VI, "‡" represents transition-state quantities. $Q_{tr}^{\ddagger}$ is the product of the translational and rotational partition functions of the transition state associated with the association process a. E_a^0 is the energy barrier with respect to reactants for the process a at 0 K; it is taken to be zero for the present case. $k_i(E)$ is the energy-specific decomposition or isomerization rate constant for the excited NH_2NO or NHNOH via step i, with $i = b, c, d, e,$ or f. $\sum P_i(E_i^{\ddagger})$ is the sum of states of the transition state i with an excess energy $E_i^{\ddagger}$ above the transition state, where i stands for transition state b, c (or d), e, or f. $N_j(E)$ is the density of states of the intermediates with $j = 1$ for NH_2NO and $j = 2$ for HNNOH. $Q_i^{\ddagger}$ and Q_j are the overall rotational partition functions for transition state i and intermediate j, with $i = b$, c (or d), e, or f; $j = 1$ or 2.

TABLE 3: Molecular Parameters Used for RRKM Calculations for the Different Channel for the NH_2 + NO Reaction[a]

channel i	$Q_i^{\ddagger}/Q_j$	$E_i^{\ddagger}$ [b]	$FR_i^{\ddagger}$ [c]	$\nu_i^{\ddagger}$/cm^{-1}
b	2.78	$E_b^{\ddagger}$	10(2)	3200 (2), 1900, 1500, 200 (2)
c	1.86	$E_b^{\ddagger}$ +14.4	0	3791, 2160, 1602 (2), 1348, 1006, 1207, 629
d	0.81	$E_b^{\ddagger}$ +14.4		
e	1.28	$E_b^{\ddagger}$ +7.4	5(1)	3700, 3000, 1300 (2), 900 (3)
f	1.10	$E_b^{\ddagger}$ +1.0	0	4030, 3680, 1793, 1194, 585 (2), 389, 344

[a] The vibrational frequencies of the intermediates provided by Walch[35] are listed as follows (in cm^{-1}). NH_2NO: 3871, 3490, 1792, 1709, 1368, 1207, 712, 647, 542. HNNOH: 3757, 3296, 1651, 1462, 1366, 884, 637, 970, 364. [b] $E_i^{\ddagger}$ is the excess energy (in kcal mol^{-1}) above the zero-point energy of the transition state i at total energy E; $E_b^{\ddagger}$ is the excess energy above the entrance transition state. [c] $FR_i^{\ddagger}$ stands for averaged moments of inertia (in 10^{-40} g cm^2) for free internal rotations of the transition state i with degeneracies in parentheses. The imaginary frequencies of all transition states are not included in the table.

Table 3 lists the molecular properties of the adducts and transition states used in the RRKM calculation. Because no quantum calculated results for loose radical–radical association transition states were available, both rotational and vibrational parameters for the transition state a (or b) and e were obtained from the fitting of experimental data at room temperature. For the transition state a, its vibrational frequencies and moment of inertia were estimated by fitting our experimental least-squares fitted rate constant at 297 K, $k_t(297) = 1.27 \times 10^{-11}$ cm^3/s. In order to account for the rather large rate constant, two free internal rotations for the transition state a were assumed. The similar procedure was employed for the transition state e by fitting the branching ratio of the channel e at room temperature, $\alpha(298) = 0.1$, which is the common experimental result obtained by Atakan et al.,[20] Bulatov et al.,[21] and Stephens et al.[23]

The results of the RRKM calculation with selected temperatures at 50 Torr of pressure are listed in Table 4. Figure 5 shows the Arrhenius plot for k_t (solid line), k_{H_2O} (single-dot dashed line), and k_{OH} (double-dot dashed line) obtained in this work. The open circles shown in the figure are our experimental results obtained by the cavity-ring-down method; two other sets of data[12,20] measured over wider temperature ranges are also included for comparison. The calculated results agree reasonably well with the experimental data, exhibiting a strong downward curvature of k_t with negative temperature dependence. Agreement in the total rate constant k_t at the low-temperature end is constrained by the parameters of the transition state a adjusted to produce the experimental data at 297 K. At higher temperatures, the calculated k_t is in good agreement with that by Atakan et al. within experimental uncertainty but slightly higher than Silver and Kolb's data obtained by the discharge flow technique. The results of our RRKM calculation also indicate that the effect of pressure on k_t is unimportant, in full agreement

TABLE 4: Calculated Values of Total and Individual Channel Rate Constants as Well as Branching Ratios for the NH_2 + NO Reaction at Selected Temperatures[a]

T/K	k_{w1}	k_{w2}	k_{OH}	k_{H_2O}	k_t	k_{OH}/k_t	$(k_{OH} + k_{H_2O})/k_t$
300	0.12	0.23	1.26	11.12	12.73	0.099	0.973
500	0.04	0.07	0.98	7.15	8.25	0.119	0.986
700	0.02	0.03	0.88	5.29	6.22	0.141	0.992
1000	0.01	0.01	0.80	3.74	4.56	0.175	0.996
1500	0.00	0.00	0.75	2.45	3.20	0.234	1.000
2000	0.00	0.00	0.73	1.83	2.56	0.285	1.000

[a] Rate constants, given in units of 10^{-12} cm^3/s, were computed at 50 Torr of pressure.

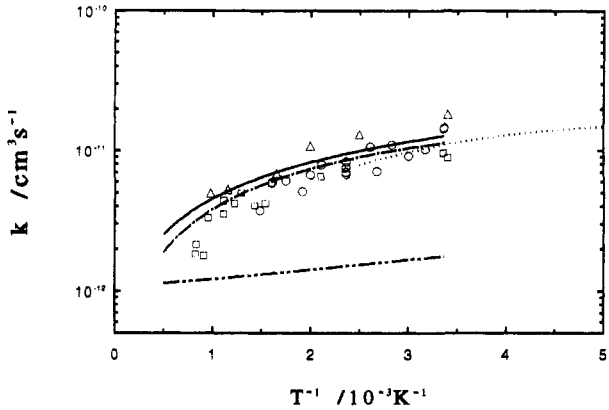

Figure 5. Comparison of the theoretical and experimental values of the second-order rate constant for the reaction NH_2 + NO. The points are experimental data of different groups: (○) this work; (△) Atakan et al.;[20] (□) Silver and Kolb.[12] The solid curve is the RRKM result for the total rate constant (k_t), the single-dot dashed curve for reaction 1, and the double-dot dashed curve for reaction 2. The dotted curve is for reaction 1 by Phillips.[47]

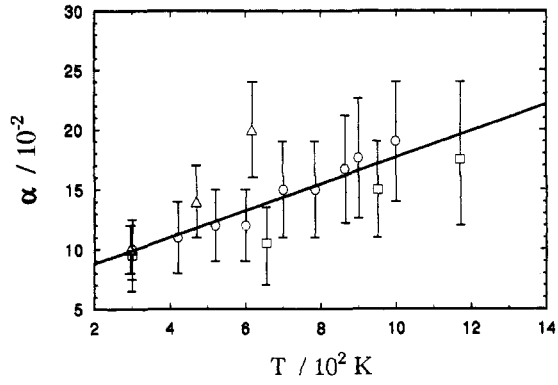

Figure 6. Comparison of the theoretical branching ratio for OH and experimental fractional OH yields as a function of temperature. The experimental data are expressed as (△) Bulatov et al.,[21] (○) Atakan et al.,[20] and (□) Stephens et al.[23] The solid line is the calculated OH branching ratio based on the RRKM theory.

with experimental findings; e.g., k_t increases by 17% at 300 K and only 3% at 1000 K, when the system pressure is increased from 1 Torr at 1 atm.

The dotted line shown in Figure 5 represents the theoretical value of k_{H_2O} reported by Phillips,[47] who calculated the capture rates of the NH_2 + NO association reaction, using a dipole–dipole + Morse potential, in conjunction with RRKM calculations for NH_2NO^* isomerization and decomposition processes based on the potential energy diagram constructed by Melius and Binkley.[33] Phillips' result is in excellent agreement with ours in the temperature range 300–400 K, where both sets of data overlap, although the collisional deactivation data of the excited intermediates were not included in his calculations.

In summary, the good agreement in the temperature dependence of k_t between the RRKM result and experimental observations is most satisfying. The computed rate constants for the two product channels and the total rate constant, in units of cm^3/s, can be given by the following equations at 50 Torr for the temperature range 300–2000 K:

$$k_{OH} = 6.6 \times 10^{-13} \exp(196/T)$$

$$k_{H_2O} = 7.9 \times 10^{-9} T^{-1.1} \exp(-98/T)$$

$$k_t = 1.6 \times 10^{-9} T^{-0.85}$$

B. Branching Ratio. The second-order rate constant for OH production is less strongly negative-temperature dependent than H_2O production, as shown in Figure 5. This means that the OH channel may become relatively more important at evaluated temperatures. Figure 6 compares the OH branching ratio (α) predicted by the RRKM theory (solid line) with those of experimental observations reported by Atakan et al.[20] (open circles), Bulatov et al.[21] (open triangles), and Stephens et al.[23] (open squares). The theoretical value of α was constrained to fit the experimental data of these three groups at room temperature by adjusting the molecular parameters of the transition state *e*, which are listed in Table 3. Our result reveals that the value of α is very sensitive to the enthalpy of reaction 2 at 0 K. Unfortunately, no experimental data are available for $\Delta H_f^0(N_2H)$ in the literature, and as mentioned previously, there have been a lot of discrepancies in the calculated values of ΔH_2^0. Recent calculations provide a value of 0.7 and 1.9 kcal mol^{-1} for ΔH_2^0 by Walch[35] and Melius,[33] respectively, with about 3 kcal mol^{-1} of uncertainty. We used −1 kcal mol^{-1} for ΔH_2^0 in our RRKM calculation to obtain the best fit to the experimental data. Repeating the same fitting procedure, with $\alpha(298) = 0.1$ but using +1 instead of −1 kcal mol^{-1} for ΔH_2^0, one obtains a value of $\alpha = 0.68$, instead of 0.17 at 1000 K.

The recent investigation by Stephens et al.[23] for the branching ratio of the NH_2 + NO system reveals that the sum of the OH and H_2O yields fails to account for 100% of the initial NH_2 at elevated temperatures. The $([OH] + [H_2O])/[NH_2]_0$ ratio decreases from 95% at room temperature to about 75% near 1200 K. They hypothesized that a third channel which produced neither OH nor H_2O might become significant at elevated temperatures. They also recognized that it was very difficult to propose a plausible channel to account for the experimental finding. Our RRKM calculation shows that 97% of NH_2 produces OH and H_2O at 300 K; the other 3% forms adducts, NH_2NO and HNNOH. However, the $([OH] + [H_2O])/[NH_2)]_0$ ratio should increase gradually up to 100% when temperature is raised from 300 to 1000 K, as shown in Table 4. Thus, the formation of NH_2NO and HNNOH cannot account for the loss of NH_2 at high temperatures. In order to solve the mystery, we have performed kinetic modeling in conjunction with sensitivity analysis for the NH_2 + NO reaction to examine the role of secondary processes in the apparent loss of NH_2 at high temperatures.

C. Kinetic Modeling. *OH and H_2O Yields.* The modeling was performed with CHEMKIN and SENKIN programs developed by Sandia National Laboratories.[53,54] The relevant reactions as well as their Arrhenius parameters employed to simulate NH_2, OH, and H_2O concentration–time profiles are presented in Table 5. The Arrhenius parameters for all channels

TABLE 5: Reactions and Rate Constants Used in the Modeling of the NH_2 + NO System[a]

reaction	A	B	E	ref
1. $NH_2 + NO = N_2 + H_2O$	4.7E15[h]	−1.09	186	*b*
2. $NH_2 + NO = N_2H + OH$	4.9E11	−0.03	−362	*b*
3. $NH_2 + NO = NH_2NO$	8.5E20	−3.82	1430	*b*
4. $NH_2 + NO = HNNOH$	3.4E22	−4.27	1730	*b*
5. $N_2H + M = H + N_2 + M$	1.0E14	0.0	3000	55
6. $N_2H + NO = HNO + N_2$	7.2E13	−0.4	0	*c*
7. $OH + NO + M = HONO + M$	1.6E14	0.5	0	56
8. $NH_2 + OH + M = H_2NOH + M$	5.7E24	−3.0	0	*d*
9. $NH_2 + OH = NH_3 + O$	2.0E10	0.4	500	57
10. $NH_2 + OH = NH + H_2O$	5.0E11	0.5	1980	58
11. $NH_3 + M = NH_2 + H + M$	2.2E16	0.0	93470	62, *e*
12. $N_2H_4 + M = NH_2 + NH_2 + M$	4.0E15	0.0	40930	58, *e*
13. $NH_2 + NH_2 = NH + NH_3$	5.0E13	0.0	10000	62, *e*
14. $NH + NO = N_2O + H$	See ref.			*f*
15. $NH + NO = N_2 + OH$	2.2E13	−0.23	0	66
16. $H + NO + M = HNO + M$	5.4E15	0.0	−600	59
17. $H + NO_2 = OH + NO$	4.9E12	0.5	0	58
18. $NH_2 + HONO = NH_3 + NO_2$	7.8E11	0.0	−380	*g*
19. $NH_2 + HNO = NH_3 + NO$	5.0E11	0.5	990	58
20. $NH_2 + NO_2 = N_2O + H_2O$	1.2E12	0.0	−1290	60
21. $NH_2 + NO_2 = N_2 + H_2O_2$	6.3E10	0.0	−1290	60
22. $OH + NH_3 = H_2O + NH_2$	2.0E12	0.0	1830	61
23. $NH_2 + H = NH + H_2$	4.0E13	0.0	3650	62
24. $NH_2 + NH = N_2H_2 + H$	1.5E15	−0.5	0	62
25. $OH + HONO = H_2O + NO_2$	7.8E11	0.0	−380	63
26. $H + H + M = H_2 + M$	5.0E18	−1.0	0	58
27. $H + OH + M = H_2O + M$	1.8E22	−1.5	0	58
28. $H + HNO = H_2 + NO$	4.5E11	0.72	650	64
29. $OH + H_2 = H_2O + H$	6.4E6	2.0	12400	65
30. $OH + HNO = H_2O + NO$	1.1E13	0.0	0	64
31. $OH + OH = H_2O + O$	2.2E8	1.4	−400	65
32. $OH + OH + M = H_2O_2 + M$	5.7E24	−3.0	0	65
33. $OH + NH = N + H_2O$	5.0E11	0.5	2000	58
34. $OH + NH = HNO + H$	5.0E11	0.5	2000	58
35. $HNO + 2NO = HN_2O + NO_2$	1.7E11	0.0	2100	64
36. $HN_2O + NO = HN_2 + NO_2$	3.2E12	0.0	540	64
37. $HN_2O + NO = N_2 + HONO$	2.6E11	0.0	1620	64

[a] The tabulated rate constants are defined by $k = AT^B \exp(-E/RT)$, where E is in cal mol^{-1} and the bimolecular rate constants are in cm^3 mol^{-1} s^{-1}. The equal sign in each reaction indicates that both forward and reverse reactions are included in the modeling. [b] This work, P = 19 Torr. [c] Estimated by the HCO + NO = HNO + CO reaction.[69] [d] Estimated by the OH + OH + M = H_2O_2 + M reaction.[65] [e] The Arrhenius parameters for the listed rate constants are only valid at high temperatures. For room temperature modeling, the following experimental data were used (in units of cm^3 mol^{-1} s^{-1}): k(H + NH_2 → NH_3) = 2.2 × 10^{12}, P = 19 Torr, T = 298 K;[7] k(NH_2 + NH_2 → N_2H_4) = 1.0 × 10^{12}, P = 19 Torr, T = 300 K;[67] k(NH_2 + NH_2 → NH + NH_3) = 2.0 × 10^9, P = 1 Torr, T = 296 K.[68] [f] k = 2.94 × 10$^{14}T^{-0.4}$−2.16 × 10$^{13}T^{-0.23}$ as recommended by Miller and Melius.[66] [g] Estimated from OH + HONO = H_2O + NO_2 reaction.[63] [h] Read as 4.7 × 10^{15}.

of the NH_2 + NO reaction, listed in Table 5 given by reactions 1–4, were obtained from our RRKM calculation. The other reactions and their rate constants were adopted from the literature as referenced. The initial conditions used to model the system were set to be the same as the experimental ones employed by Stephens et al.[23] Typically, 12 mTorr of NH_3 and 400 mTorr of NO were mixed with 18 Torr of He. The temperature was varied between 299 and 1171 K.

The only item we have not been able to ascertain in the modeling is the initial concentration of the NH_2 radical, $[NH_2]_0$, which was produced from the photodissociation of NH_3 at 193 nm. Stephens et al. assumed that the amount of NH_3 lost is equal to the amount of NH_2 produced by the photolysis of NH_3. In our modeling, we varied the amount of NH_2 from 1 to 90% of the initial NH_3 concentration, $[NH_3]_i$. Parts a and b of Figure 7 compare the simulated profiles of $[NH_2]$, [OH], and $[H_2O]$ from this modeling at T = 299 and 1171 K, respectively, with $[NH_2]_0/[NH_3]_i$ = 0.1 and 0.5. Since Stephens et al. did not indicate the initial concentration of NH_2, their OH and H_2O profiles were normalized to our calculated plateau values with $[NH_2]_0/[NH_3]_i$ = 0.1. The calculated profiles for NH_2, OH, and H_2O agree reasonably well with all the observed ones, except for H_2O at 299 K, at which the experimental curve exhibits a pronounced induction time, incompatible with those of the measured and calculated OH profiles.

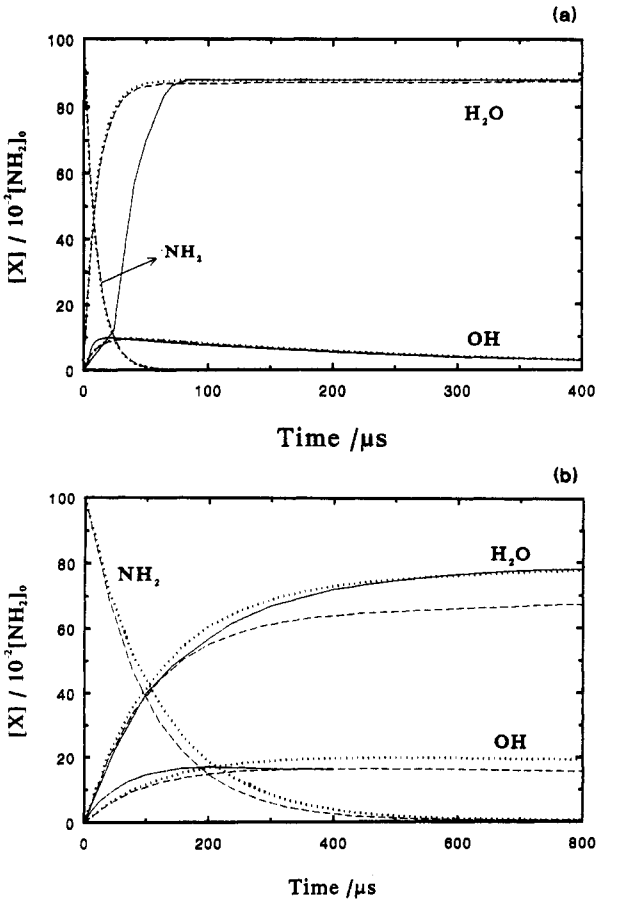

Figure 7. Kinetic modeling of temporal concentration profiles for NH_2, H_2O, and OH for the following conditions: P_{NH_3} = 12 mTorr; P_{NO} = 400 mTorr; P_{He} = 18 Torr; P_{SF_6} = 400 mTorr. The solid curves are smoothed experimental results obtained from Figures 3 and 4 of ref (23), which were normalized to the calculated plateau values for $([NH_2]_0/[NH_3]_i)$ = 0.1, for (a) 299 K and (b) 1171 K, respectively. The dotted and dashed curves are the kinetically modeled results for $[NH_2]_0/[NH_3]_i$ = 0.1 and 0.5, respectively.

To distinguish the fractional yields of OH and OH + H_2O from the OH branching ratio (α), we defined these fractional quantities as

$$\beta = [OH]_t/[NH_2]_0$$

$$\gamma = ([OH]_t + [H_2O]_t)/[NH_2]_0$$

where $[OH]_t$ and $[H_2O]_t$ are the concentrations of OH and H_2O at time t, respectively. Both β and γ are functions of time. However, it is difficult to ascertain the exact time at which Stephens et al. measured [OH] and $[H_2O]$. In a separate study, Atakan et al.[20] mentioned that [OH] was determined when its profile reached a plateau value. Our results presented in Figure 7 indeed reveal that the total fractional yield (γ) approaches a constant value in both cases shown after NH_2 has been depleted. This indicates that the total fractional yield computed in our modeling would not be affected very much by the uncertainty in time when [OH] and $[H_2O]$ were measured.

If we express the concentration of NH_3 before photolysis in the system as given above by $[NH_3]_i$, the concentrations of NH_3, NH_2, and H after photolysis at zero reaction time are $[NH_3]_0$, $[NH_2]_0$, and $[H]_0$. Then, we have the following relationship:

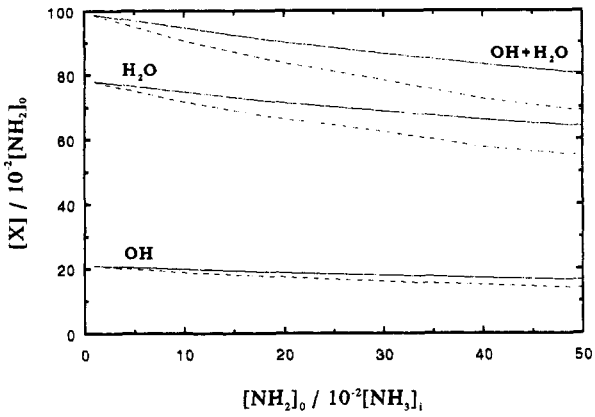

Figure 8. Kinetically modeled results for $\beta = [OH]/[NH_2]_0$, $[H_2O]/[NH_2]_0$, and $\gamma = ([OH] + [H_2O])/[NH_2]$ with the same conditions as described in Figure 7b ($T = 1171$ K) using different initial NH_2 and NH_3 ratios ($[NH_2]_0/[NH_3]_i$). The dashed curves are the modeled data under the same conditions but with the values of the rate constants for reactions 23 and 13 doubled.

$$[NH_3]_i = [NH_3]_0 + [NH_2]_0$$

$$[NH_2]_0 = [H]_0$$

In order to elucidate the importance of $[NH_2]_0$ in this system, we calculated the values of β and γ as functions of $[NH_2]_0/[NH_3]_i$ for the two extreme temperatures studied by Stephens et al.; that is, to keep the initial conditions the same except the proportion of $[NH_2]_0$ in $[NH_3]_i$ for each modeling calculation. The modeled results with $T = 1171$ K are shown in Figure 8. This modeling manifests clearly that higher $[NH_2]_0$ will result in more serious secondary reactions at elevated temperatures and thus reduce the value of γ (also β slightly) observed in the experiment. The room temperature modeling only shows a small change in both β and γ with $[NH_2]_0$. This may be understood by the negative temperature effect of the $NH_2 + NO$ system. Even though the $[NH_2]_0$ is as high as 4×10^{14} molecules cm^{-3} (12 mTorr at 299 K), secondary reactions do not contribute significantly at room temperature. But when the temperature was raised to 1171 K, the total reaction rate constant (k_t) for $NH_2 + NO$ decreased to about 20% of the value at room temperature. On the other hand, several key secondary reactions, which have rate constants with positive temperature dependence, become more important at 1171 K when $[NH_2]_0$ is larger. The effect of secondary reactions at high temperatures on the values of β and γ will be discussed below according to the results of sensitivity analyses.

H Atom Production. The yield of hydrogen atoms from the $NH_2 + NO$ reaction has been the subject of much interest because H atoms can be produced directly from channel 2

$$NH_2 + NO \rightarrow H_2NNO \rightarrow HNNOH \rightarrow H + N_2 + OH$$

with an overall exothermicity of about 7 kcal/mol. If H atoms are produced directly from this reaction, one would intuitively expect a higher [H] than from the alternative N_2H production mechanism.

There have been two attempts to measure the yield of H atoms from the above reaction. Silver and Kolb[12] employed the H atom Lyman-α resonance absorption method to monitor the production of H atoms using NH_2 generated by the $F + NH_3$ reaction. Since no H atoms were present initially, any H atoms formed in the reaction would be readily detected with a sensitivity of 2.5×10^{10} molecules/cm^3. Interestingly, they detected no noticeable absorption of the Lyman-α line by H atoms in the experiment. The result of our kinetic modeling using their typical initial conditions—$[NH_3]_0 = 2 \times 10^{12}$, $[NH_2]_0 = 5 \times 10^{11}$, $[NO] = 5.7 \times 10^{13}$ molecules/cm^3 at $T = 298$ K and P = 1.15 Torr—indicated that, regardless of the mechanisms assumed (i.e., N_2H vs $N_2 + H$), the maximum yield of H atoms is about 4×10^{10} molecules/cm^3, which is slightly higher than their detection limit. It is expected, however, that losses by wall-catalyzed self-recombination and with NO under the low-pressure conditions employed may reduce it to near or below the detection limit.

The second attempt to detect H atoms was made by Andresen et al.[14] in a wide temperature range of 290–900 K, also with the H Lyman-α resonance absorption method. The yield of H atoms from $NH_2 + NO$ was found to be ≤ 0.05, i.e., less than or equal to 5% of the H atoms already present from the photodissociation of NH_3, the source of NH_2. The result of the kinetic modeling, using their typical conditions—$[NH_3]_i = 4.8 \times 10^{12}$, $[H]_0 = [NH_2]_0 = 4.8 \times 10^{11}$, $[NO] = 5.4 \times 10^{13}$ molecules/cm^3 at $T = 898$ K and $P = 5$ Torr—suggests that the maximum yield of H atoms is only 6.8% higher than the initial value, again independent of the mechanisms, N_2H vs $N_2 + H$, assumed for reaction 2. These results clearly suggest that the low yield of H atoms measured experimentally does not allow us to rule out the possibility of their direct production from reaction 2, although it is kinetically less favored.

HNO Formation. The formation of HNO is also directly related to reaction 2. HNO can be produced by the following two key processes:

$$N_2H + NO \rightarrow HNO + N_2 \quad (6)$$

$$H + NO + M \rightarrow HNO + M \quad (16)$$

Unfried et al.[22] attempted to measure HNO with an infrared diode laser using a 52-m multiplass reactor at room temperature. On the basis of their measurement using the $CHO + NO \rightarrow HNO + CO$ calibration reaction, they concluded that $\leq 1\%$ of NH_2 was converted to HNO from the $NH_2 + NO$ reaction. The result of our calculation using the starting conditions $[NH_3]_i = 3.89 \times 10^{15}$, $[NH_2]_0 = [H]_0 = 3.89 \times 10^{14}$, $[NO] = 3.24 \times 10^{15}$ molecules/cm^3 at $T = 298$ K and $P = 19.8$ Torr gives $[HNO]_{max}/[NH_2]_0 = 1.2\%$, which is in agreement with the experimental finding. This modeling also shows that about 66% of the HNO derived from reaction 16, $H + NO + M$, and the remaining contribution from reaction 6, $N_2H + NO$ (at $t = 100$ μs). The assumption of the direct H atom production from reaction 2 reduced the ratio $[HNO]_{max}/[NH_2]_0$ to $<0.6\%$. Interestingly, the measurement of HNO yields from the $NH_2 + NO$ reaction appears to be ineffective in differentiating the mechanism of reaction channel 2, one of the objectives in Unfried's study.[22]

D. Sensitivity Analyses. The effect of all reactions presented in Table 5 on the disappearance of NH_2 and the formation of the two major products, H_2O and OH, has been systematically studied by sensitivity analysis using the SENKIN program.[54] In order to identify the secondary reactions occurring in the $NH_2 + NO$ system, the same conditions as discussed in the previous section were used to perform this analysis.

Our analysis reveals that at room temperature the major contributors to the disappearance of NH_2 are reactions 1 and 2, as one would expect. Minor processes which also affect the loss of NH_2 are reactions 3 and 4; however, they become less effective above room temperature. There are two other side association reactions, (−11) and (−12), which form NH_3 and N_2H_4, respectively, that contribute slightly to the NH_2 loss when $[NH_2]_0$ is high (i.e., $[NH_2]_0 = 0.5[NH_3]_i$). Similar sensitivity results were obtained for the production of H_2O and OH. These results, combined with the data shown in Figure 7a, lead us to conclude that reactions 1 and 2 contribute 96% of the NH_2 loss at low $[NH_2]_0$ (i.e., $[NH_2]_0/[NH_3]_i = 0.01$) at 299 K, and the remaining 4% loss results from reactions 3 and 4; this is an expected result from our RRKM calculation. At very high NH_2 concentrations (e.g., $[NH_2]_0/[NH_3]_i = 0.9$), the result is essentially the same; about 93% of the NH_2 loss comes from reactions 1 and 2, and

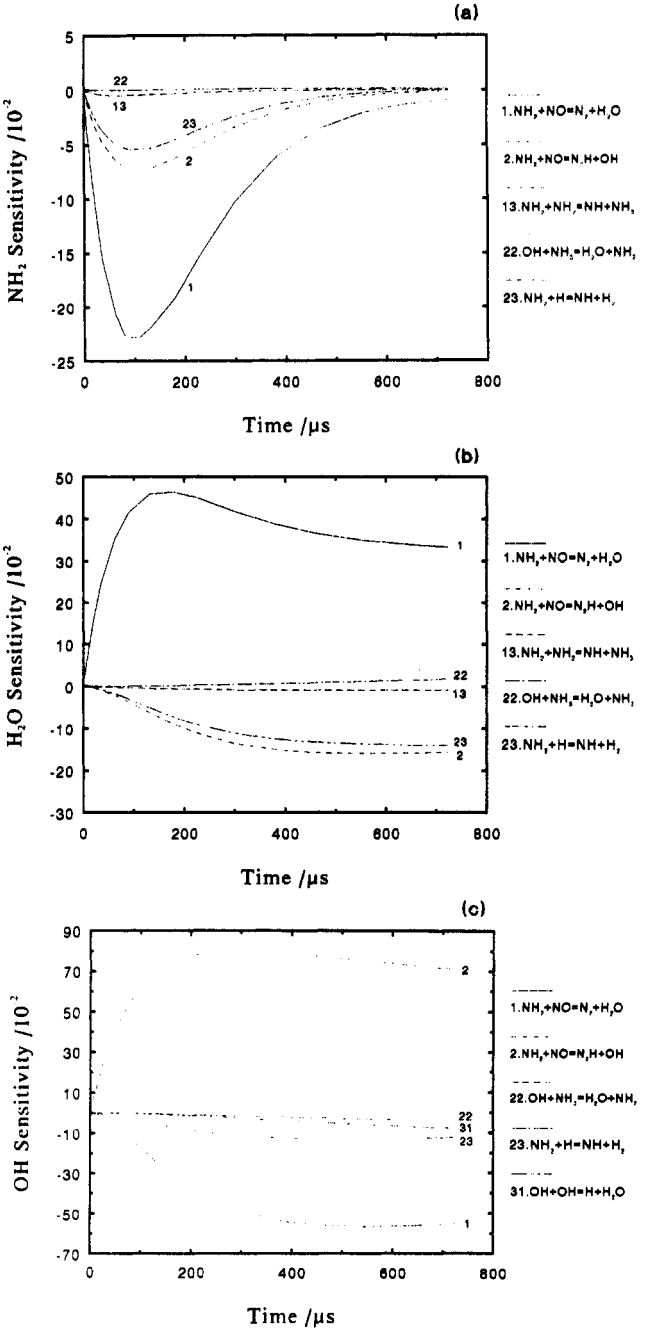

Figure 9. Normalized sensitivity coefficients of the key reactions at 1171 K and $([NH_2]_0/[NH_3]_i) = 0.5$ for (a) NH_2, (b) H_2O, and (c) OH.

the remaining 7% comes from reactions 3, 4, −11, and −12, among them approximately a half of the loss from reactions −11 and −12.

When the system temperature was raised to 1171 K, the result of our sensitivity analysis predicted that none but reactions 1 and 2 were dominant under low $[NH_2]_0$ conditions. At this temperature, reactions 3 and 4 are no longer relevant as can be seen from the RRKM result presented in Table 4. Under high $[NH_2]_0$ conditions, on the other hand, many secondary reactions can contribute to the loss of NH_2 without producing either OH or H_2O. The result summarized in Figure 8 shows the effect of the secondary reactions on β as the conversion of NH_3 is increased.

Figure 9a presents the normalized sensitivity coefficients for several major reactions which affect the concentration of the NH_2 radical. It is clear that aside from reactions 1 and 2, reaction 23 also contributes noticeably to the loss of NH_2 under the conditions of $[NH_2]_0/[NH_3]_i = 0.5$ and $T = 1171$ K. Reaction 23 produces NH, which is also important in the thermal de-NO_x process. A further analysis for NH reveals that NH disappears primarily by its reaction with NO to form N_2O + H. Reaction 22, which consumes OH by reacting with NH_3 to regenerate the reactant NH_2, gives a slightly positive contribution to the NH_2 sensitivity coefficient. For the formation of H_2O, the normalized sensitivity coefficients for the most dominant reactions are shown in Figure 9b. Aside from reactions 1 and 2, which are competitive with different signs as expected, reaction 23 is again most negatively influential because it depletes the NH_2 radical. The sensitivity coefficients for OH are shown in Figure 9c. For obvious reasons, the primary reaction 2 has a positive effect on its production. Similarly, reactions 1, 23, and 31 are expected to have a negative effect on OH concentration.

To conclude, on the basis of the results of these sensitivity analyses, one can infer that the loss of NH_2 by the mysterious "third channel" may result, at least in part, from several secondary NH_2 reactions, such as

$$NH_2 + H \rightarrow NH + H_2 \quad (23)$$

$$NH_2 + NH_2 \rightarrow NH + NH_3 \quad (13)$$

which do not produce either OH or H_2O at high temperatures. The decrease in the value of $\gamma = ([OH] + [H_2O])/[NH_2]_0$ at higher temperatures could indeed be simulated, at least qualitatively, by kinetic modeling using the rate constants currently available in the literature.

Since the rate constants for reactions 23 and 13 were evaluated mainly from high-temperature ($T > 2000$ K) kinetic modeling,[62] the use of these rate constants at 1000 K by extrapolation tends to underestimate their contributions significantly because of the upward curvature of bimolecular rate constants at high temperatures. In order to test that effect, we doubled the values of these rate constants at 1173 K; the calculated results for OH and H_2O, as represented by the dashed curves in Figure 8, are noticeably lower. Accordingly, in order to quantitatively account for the change in the value of the $\gamma = ([OH] + [H_2O])/[NH_2]_0$ ratio, we need more accurate determinations for these secondary reactions near 1000 K. For reaction 23, the literature values vary by as much as a factor of 10 at 2500 K.[62]

In addition to the kinetic modeling and sensitivity analyses, we have successfully interpreted the effect of temperature on the total rate constant for the NH_2 + NO reaction and its OH/H_2O product branching ratio using the potential energy surface data of Walch,[35] in conjunction with a multichannel RRKM calculation.

Acknowledgment. We gratefully acknowledge the Office of Naval Research for support of this work through Contract N00014-89-J1949 and the Cherry L. Emerson Center for Computation Science for the use of an IBM RISC 6000 system. M. A. G. Wagner acknowledges the award of a GIFT fellowship. We also express our deep gratitude to Ms. Fran Rupley of Sandia National Laboratories for providing us with a UNIX version of the CHEMKIN and SENKIN programs as well as for her generous help in solving the initial I/O problems. Useful discussions with Dr. C. E. Kolb on the controversy regarding H atom production and the input of Ms. Cheryl Morter as well as Professor G. P. Glass on their experimental conditions are much appreciated.

References and Notes

(1) McConnell, J. C. *J. Geophys. Res.* **1973**, *78*, 7812.
(2) Logan, J. A.; Prather, M. J.; Wofsy, S. C.; McElroy, M. B. *J. Geophys. Res.* **1981**, *86*, 7210.
(3) Gardiner, W. C., Jr.; Olson, D. B. *Annu. Rev. Phys. Chem.* **1980**, *31*, 377.
(4) Lyon, R. K. U.S. Patent 3,900,554.
(5) Lyon, R. K. *Int. J. Chem. Kinet.* **1976**, *8*, 315.

(6) Miller, J. A.; Branch, M. C.; Kee, R. J. *Combust. Flame* **1981**, *43*, 81.
(7) Gordon, S.; Mulac, W.; Nangia, P. *J. Phys. Chem.* **1971**, *75*, 2087.
(8) Gehring, M.; Hoyermann, K.; Schacke, H.; Wolfrum, J. *14th Symp. (Int.) on Combustion*; Combustion Institute: Pittsburgh, 1973; p 99.
(9) Hancock, G.; Lange, W.; Lenzi, M.; Welge, K. H. *Chem. Phys. Lett.* **1975**, *33*, 168.
(10) Lesclaux, R.; Khê, P. V.; Dezauzier, P.; Soulignac, J. C. *Chem. Phys. Lett.* **1975**, *35*, 493.
(11) Hack, W.; Schacke, H.; Schröter, M.; Wagner, H. Gg *17th Symp. (Int.) on Combustion*; Combustion Institute: Pittsburgh, 1979; p 505.
(12) Silver, J. A.; Kolb, C. E. *J. Phys. Chem.* **1982**, *86*, 3240.
(13) Stief, L. J.; Brobst, W. D.; Nava, D. F.; Borkowski, R. P.; Michael, J. V. *J. Chem. Soc., Faraday Trans. 2* **1982**, *78*, 1391.
(14) Andresen, P.; Jacobs, A.; Kleinermanns, C.; Wolfrum, J. *19th Symp. (Int.) on Combustion*; Combustion Institute: Pittsburgh, 1983; p 11.
(15) Whyte, A. R.; Phillips, L. F. *Chem. Phys. Lett.* **1983**, *102*, 451.
(16) Gericke, J.-H.; Torres, L. M.; Guillory, W. A. *J. Chem. Phys.* **1984**, *80*, 6134.
(17) Dreier, T.; Wolfrum, J. *20th Symp. (Int.) on Combustion*; Combustion Institute: Pittsburgh, 1985; p 695.
(18) Hall, J. L.; Zeitz, D.; Stephens, J. W.; Kasper, J. V. V.; Glass, G. P.; Curl, R. F.; Tittel, F. K. *J. Phys. Chem.* **1986**, *90*, 250.
(19) Dolson, D. A. *J. Phys. Chem.* **1986**, *90*, 6714.
(20) Atakan, B.; Jacobs, A.; Wahl, M.; Weller, R.; Wolfrum, J. *Chem. Phys. Lett.* **1989**, *155*, 609.
(21) Bulatov, V. P.; Ioffe, A. A.; Lozovsky, V. A.; Sarkisov, O. M. *Chem. Phys. Lett.* **1989**, *161*, 141.
(22) Unfried, K. G.; Glass, G. P.; Curl, R. F. *Chem. Phys. Lett.* **1990**, *173*, 337.
(23) Stephens, J. W.; Morter, C. L.; Farhat, S. K.; Glass, G. P.; Curl, R. F. *J. Phys. Chem.* **1993**, *97*, 8944.
(24) Salimian, S.; Hanson, R. K. *Combust. Sci. Technol.* **1980**, *23*, 225.
(25) Silver, J. A. *Combust. Flame* **1983**, *53*, 17.
(26) Miller, J. A.; Smooke, M. D.; Green, R. M.; Kee, J. R. *Combust. Sci. Technol.* **1983**, *34*, 149.
(27) Salimian, S.; Hanson, R. K.; Kruger, C. H. *Combust. Flame* **1984**, *56*, 83.
(28) Dearn, A. M.; Chou, M. S.; Stern, D. *Int. J. Chem. Kinet.* **1984**, *16*, 633.
(29) Kimball-Linne, M. A.; Hanson, R. K. *Combust. Flame* **1986**, *64*, 377.
(30) Silver, J. A.; Kolb, C. E. *J. Phys. Chem.* **1987**, *91*, 3713.
(31) Goddard, W. A., III; Casewit, C. J. *J. Am. Chem. Soc.* **1982**, *104*, 3280.
(32) Abou-Rachid, H.; Pouchan, C.; Chaillet, M. *Chem. Phys.* **1984**, *90*, 243.
(33) Melius, C. F.; Binkley, J. S. *20th Symp. (Int.) on Combustion*; Combustion Institute: Pittsburgh, 1985; p 575.
(34) Harrison, J. A.; Maclagan, G. A. R.; Whyte, A. R. *J. Phys. Chem.* **1987**, *91*, 6683.
(35) Walch, S. P. *J. Chem. Phys.* **1993**, *99*, 5295.
(36) Lathan, W. A.; Curtiss, L. A.; Hehre, W. J.; Lisle, J. B.; Pople, J. A. *Prog. Phys. Org. Chem.* **1974**, *11*, 175.
(37) Vasudevan, K.; Payerimhoff, S. D.; Buenker, R. J. *J. Mol. Struct.* **1975**, *29*, 285.
(38) Baird, N. C. *J. Chem. Phys.* **1975**, *62*, 300.
(39) Baird, N. C.; Kathpal, H. B. *J. Chem. Phys.* **1977**, *55*, 863.
(40) Casewit, C. J.; Goddart, W. A. *J. Am. Chem. Soc.* **1980**, *102*, 4057.
(41) Curtiss, L. A.; Drapcho, D. L.; Pople, J. A. *Chem. Phys. Lett.* **1984**, *103*, 437.
(42) Jensen, H. J. A.; Jørgensen, P.; Helgaker, T. *J. Chem. Phys.* **1986**, *85*, 3917.
(43) Walch, S. P.; Duchovic, R. J.; Rohlfing, C. M. *J. Chem. Phys.* **1989**, *90*, 3230.
(44) Walch, S. P. *J. Chem. Phys.* **1990**, *93*, 2384.
(45) Koizumi, H.; Schatz, G. C.; Walch, S. P. *J. Chem. Phys.* **1991**, *95*, 4130.
(46) Gilbert, R. G.; Whyte, A. R.; Phillips, L. F. *Int. J. Chem. Kinet.* **1986**, *18*, 721.
(47) Phillips, L. F. *Chem. Phys. Lett.* **1987**, *135*, 269.
(48) Yu, T.; Lin, M. C. *J. Am. Chem. Soc.* **1993**, *115*, 4371.
(49) Lin, M. C.; Yu, T. *Int. J. Chem. Kinet.* **1993**, *25*, 875.
(50) Lin, M. C.; He, Y.; Melius, C. F. *Int. J. Chem. Kinet.* **1992**, *24*, 489.
(51) Lin, M. C.; He, Y.; Melius, C. F. *J. Phys. Chem.* **1993**, *97*, 9124.
(52) Troe, J. *J. Phys. Chem.* **1979**, *83*, 114.
(53) Kee, R. J.; Rupley, F. M.; Miller, J. A. *CHEMKIN-II*: A FORTRAN Chemical Kinetics Package, for the Analysis of Gas-Phase Chemical Kinetics; Sandia National Laboratory Report No. SAND89-8009, 1989.
(54) Lutz, A. E.; Kee, R. J.; Miller, J. A. *SENKIN*: A FORTRAN Program for Predicting Homogeneous Gas-Phase Chemical Kinetics with Sensitivity Analysis; Sandia National Laboratory, Report No. SAND87-8248, 1988.
(55) Mertens, D. J.; Chang, A. Y.; Hanson, R. K.; Bowman, C. T. *Int. J. Chem. Kinet.* **1989**, *21*, 1049.
(56) DeMore, W. B.; Sander, S. P.; Hampson, R. F.; Kurylo, M. J.; Golden, D. M.; Howard, C. J.; Ravishankara, A. R.; Molina, M. J. *Chemical Kinetics and Photochemical Data for Use in Stratospheric Modeling*; Evaluation No. 9, Publication 90-1; Jet Propulsion Laboratory: Pasadena, CA, 1990.
(57) Baulch, D. L.; Cobos, C. J.; Cox, R. A.; Esser, C.; Frank, P.; Just, Th.; Kerr, J. A.; Pilling, M. J.; Troe, J.; Walker, R. W.; Warnatz, J. *J. Phys. Chem. Ref. Data*, **1992**, *21*, 565.
(58) Hanson, R. K.; Salimian, S. *Combustion Chemistry*; Gardiner, E. C., Jr., Ed.; Springer-Verlag: New York, 1986; Chapter 6.
(59) Westley, F. *Table of Recommended Rate Constants for Chemical Reactions Occurring in Combustion*; NSRDS-NBS67; National Bureau of Standards: Washington, DC, 1980.
(60) Atkinson, R.; Baulch, D. L.; Cox, R. A.; Hampson, R. F., Jr.; Kerr, J. A.; Troe, J. *J. Phys. Chem. Ref. Data* **1992**, *18*, 1194.
(61) Diau, E. W.-G.; Tso, T.-L.; Lee, Y.-P. *J. Phys. Chem.* **1990**, *94*, 5261.
(62) Davidson, D. F.; Kohse-Höinghaus, K.; Chang, A. Y., Hanson, R. K. *Int. J. Chem. Kinet.* **1990**, *22*, 513.
(63) He, Y.; Kolby, E.; Shumaker, P.; Lin, M. C. *Int. J. Chem. Kinet.* **1989**, *21*, 1015.
(64) Lin, M. C.; He, Y.; Melius, C. F. *Int. J. Chem. Kinet.* **1992**, *24*, 489.
(65) Tsang, W.; Hampson, R. F. *J. Phys. Chem. Ref. Data* **1986**, *15*, 1087.
(66) Miller, J. A.; Melius, C. F. *24h Symp. (Int.) on Combustion*; Combustion Institute: Pittsburgh, 1993; p 719.
(67) Khê, P. V.; Soulignac, J. C.; Lesclaux, R. *J. Phys. Chem.* **1977**, *81*, 210.
(68) Dransfeld, P.; Hack, W.; Kurzke, H.; Temps, F.; Wagner, H. G. *20th Symp. (Int.) on Combustion*; Combustion Institute: Pittsburgh, 1985; p 655.
(69) He, Y.; Sanders, W. A.; Lin, M. C. *J. Phys. Chem.* **1988**, *92*, 5474.